SAND2017-0636J

Image quality, meteorological optical range, and fog particulate number evaluation using Sandia National Laboratories fog chamber

Gabriel C. Birch[a], Bryana L. Woo[a], Andres L. Sanchez[a], and Haley Knapp[a]
[a]Sandia National Laboratories, P.O. Box 5800 MS 0781, Albuquerque, New Mexico 87185, United States

Abstract. Testing of optical system performance in fog conditions typically requires field testing, which can be challenging due to the unpredictable nature of fog generation and the temporal and spatial non-uniformity of the phenomenon itself. We describe the Sandia National Laboratory fog chamber, a new test facility which enables the repeatable generation of fog within a 55 m x 3 m x 3 m (LxWxH) environment, and demonstrate the fog chamber through a series of optical tests. These tests are performed to evaluate image quality, determine meteorological optical range (MOR), and measure number of particles in the atmosphere. Relationships between typical optical quality metrics, MOR values, and total number of fog particles are described using the data obtained from the fog chamber, and repeated over a series of three tests.

Keywords: FIX.

Address all correspondence to: Gabriel C. Birch, Sandia National Laboratories, P.O. Box 5800 MS 1004, Albuquerque, New Mexico 87185, United States; Tel: +1 505-844-1888; E-mail: gcbirch@sandia.gov

1 Introduction

Reduced visibility due to the presence of fog can impact the performance of an imaging system significantly. Understanding these performance degradations affects many diverse areas of engineering, from aviation to physical security. We report on a newly developed fog generation test facility, and optical testing performed within this facility. Constructed at Sandia National Laboratory, the fog generation facility consists of a 55 m x 3 m x 3 m chamber capable of generating fog conditions through the spraying of water mixed with user-specified seeding chemicals.

In this study, we utilize NaCl seeded water mixtures to evaluate imaging system performance in a simulated coastal fog. We report on measurements of relative spatial frequency response (SFR) area under curve (AUC), meteorological optical range (MOR), and total number of fog particles present within the test chamber. All values are measured in one second temporal periods. A commercial security camera was used to record imagery throughout testing, in conjunction with a Malvern Spraytec particle sizer instrument measuring number of fog particles in the test chamber.

This document begins by discussing past simulations, tests, and test facilities used to examine the impact of fog on optical system performance. A description of the Sandia fog chamber is provided as well as details regarding instrumentation used to measure fog particle size distribution. MOR as an imaging metric is discussed and detail regarding utilization of a sinusoidal Siemens star test target to measure imaging system SFR is included. Three fog chamber tests at varying distances and fog densities are discussed. Relationships between the relative SFR AUC, MOR, and fog particle number quantities are found to follow expected behavior; however, relative SFR AUC was found to recover much faster than would be expected based off of MOR measurements while fog was dissipating.

2 Background

Dispersive media's effect on light propagation poses distinct challenges in many fields. Several studies focus on light propagation through obscurants and its effect on automobile safety, optical communication, and the modulation transfer function (MTF) of optical systems.[1–6] Other studies have examined the effect of wavelength on light penetration through dispersive media.[7–9] Simulations have been utilized to examine foundational aspects of photon propagation through scattering media,[10–14] but these studies often assume model parameters such as monodispersed droplet size and homogeneous atmospheric conditions.[1,15]

Validating models and measuring performance degradations typically involve field testing within naturally occurring fog.[1,6] However, evaluating system performance through field testing can prove challenging due to the temporally unpredictable behavior of naturally occurring environmental conditions such as fog.[16] In the instances where natural fog occurs in the appropriate density for the desired test, it is difficult to collect composition data such as uniformity or number and size

of particles, especially at multiple points along a testing path. The dissipation of the fog may also result in incomplete or inconsistent data with which to compare. Alternatively, the physical testing for fog can be implemented in controlled laboratory environments[17,18] through the creation of fog chambers.

An early fog chamber was created by Houghton in 1931 using wooden containers of 0.3 m x 0.025 m x 0.025 m with detectors and light sources at either end.[19] This early fog chamber experienced many of the challenges present in natural fog testing, including instability and rapid particulate dissipation, and made exact fog densities difficult to replicate due to dependence on the surrounding atmosphere.[19] Recent fog chambers include the 22 m x 2.4 m x 2.4 m Defense Research Establishment Valcartier (DREV) fog chamber located in Canada. This chamber uses a series of six fans located on the floor to distribute particulates, and permits users to simulate scattering environments with materials such as water, talcum powder, and Dualite MS3™ powder. Located outdoors, the chamber has entrances on either end that open to expose the fog or dust for testing. A Malvern Spraytec particle size analyzer is used for monitoring the fog concentrations and droplet size within this facility.[18]

An additional fog generation and testing facility was created by the Federal Aviation Administration using a 249.9 m x 9.14 m x 3.04-9.14 m indoor glide facility, located at the University of California, Berkley. The chamber was divided into 24 sections and allowed for different densities of fog in each section. The fog was created by atomizing water as it moved through an air pressurized nozzle.[20] This chamber, however, is no longer in use.[2] A more recent fog chamber was built by the European Union (EU) in France to allow public industry a place to test equipment in fog conditions. The EU fog chamber is 30 m x 5.5 m x 2 m meters and located outdoors similar to the DREV chamber. Desired visibility is reached by filling the chamber to a very dense fog then

allowing natural dissipation to occur until the appropriate visibility level is reached. In order to stabilize the fog a the desired density, small bursts of water are added to the chamber to compensate for particulate evaporation and fall out. The stabilization process applied to the EU chamber allows a consistent, dense fog to be maintained regardless of outside conditions. Though the dense fog is able to be stabilized, light fog still dissipates quickly. This chamber is mainly used for testing automotive lights and street sign visibility in fog.[2] Other smaller fog chambers have been created, including the Electro-Optical Test Facility fog chamber[21] and the VALEO Bobigny fog chamber.[17]

Along with these fog generation facilities, there are chambers designed for the production of clouds. The 30 cubic meter, high-flow turbulent cloud chamber, located in the Netherlands, has the ability to make stable, reproducible clouds that can last for hours. The cloud is formed by supersaturating the atmosphere using a humidifier and then creating a temperature difference between two areas. This chamber is primarily used to evaluate how pollutants in the air affect rain formation from clouds. Seeding the air with ammonium sulfate and sodium sulfate causes the water droplets to form around the molecules giving the cloud different physical and chemical properties than a pure water seed.[22]

These fog generation and testing facilities each provide unique capabilities relevant to their primary scientific utilization. However, the available capabilities of these chambers do not overlap. There is a need for a long-path, controlled fog generation facility capable of measuring atmospheric particulates during a test. Additionally, an idealized facility would be capable of seeding aqueous solution with differing chemical constituents to mimic unique environmental conditions including fog, pollutant haze, or mist.

The Sandia National Laboratory (SNL) Fog Generation Test Facility was designed to meet these specifications, with the primary facility purpose being the evaluation of imaging and laser-

based devices in a variety of simulated atmospheric conditions. In the remaining body of this work, we demonstrate this fog generation facility by evaluating visible imager performance and fog particulate values over time.

3 Methodology

A testing facility and method used to evaluate visible imager performance is described. Specific attributes of the Sandia National Laboratories fog chamber, as well as techniques used to collect particle size distribution data are included in section 3.1. A proof-of-concept test was performed evaluating the fog chamber using two optical performance metrics: evaluation of visible imager relative spatial frequency response area under curve changes versus number of fog particles, and measured meteorological optical range degradations versus number of fog particles. Subsection 3.2 describes how meteorological optical range degradations were measured. Subsection 3.3 describes the utilization of a sinusoidal Siemens star test target to measure relative spatial frequency response area under curve. Finally, the proof-of-concept tests are described in subsection 3.4.

3.1 Fog generation test facility

The Sandia National Laboratories (SNL) fog chamber, shown in figure 1, is approximately 55 m x 3 m x 3 m (LxWxH). The test facility purpose is primarily to test and evaluate optical systems, such as visible cameras, thermal imagers, or laser-based devices, within a stable laboratory environment. The SNL Fog Chamber has the capability to utilize differing chemical constituents to seed fog mixture with environmentally relevant products using sixty-four two-fluid air-atomizing nozzles. In this proof-of-concept test, the simulated fog was seeded with a 10 g/L NaCl salt water mixture. NaCl was chosen to closely mimic the primary constituent found in naturally forming sea

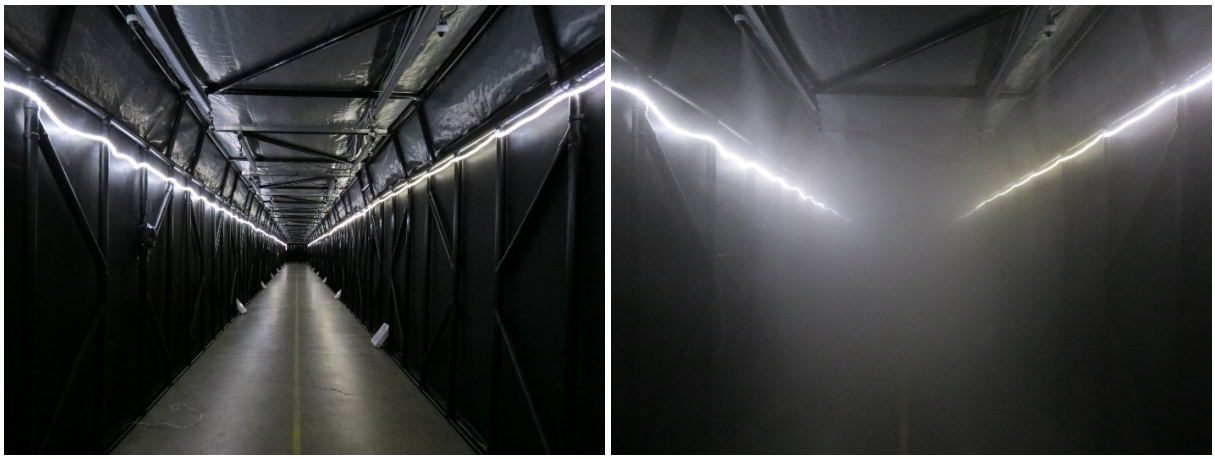

(a) (b)

Fig 1 (a) SNL Fog Chamber under nominal conditions, and (b) SNL Fog Chamber with simulated coastal fog. Safety LED lights were kept on in these images to demonstrate the scattering nature of the generated fog. However, subsequent tests removed all sources of illumination except for the test source located within the test target chamber.

coastal fog.[23–25] The chamber is separated into three sections, which enable varying fog density and particulate concentrations. However, for the purposes of test consistency, all sections were run with the same nozzle conditions; air flow rate of 3-4 cubic feet per minute and liquid flow rate of 115 mL/minute.

Particle size distribution is measured in one second intervals using a Malvern Spraytec instrument and inhalation cell accessory. The Malvern Spraytec instrument calculates particle size, which is inversely proportional to scattering angle, via indirect measurements of light scatter off particulates onto a detector. Mie theory, which predicts absorption and light scatter intensity of a spherical particle, is the fundamental model which the Malvern software utilizes to determine particle size.[24,26,27] Additionally, the inhalation cell accessory was used as an enclosed measurement zone with a controlled sample flow rate. This is important for particle size accuracy and post-measurement concentration calculations, which utilizes the Beer-Lambert Law and particle diameter to determine volume concentration. Accuracy of the particle size measurements were verified using the wet dispersion cell accessory and NIST traceable standards. Verification was de-

termined by the manufacturer by taking measurements of three different polystyrene latex sphere sizes at 40μm, 9μm, and 1μm). The Malvern instrument correctly predicted test particle size to within $\pm 1\%$ accuracy.

During data collection, the Malvern Spraytec calculates particle size measurements as volume-based results. Restated, each particle size bin consists of a derived percentage of the total volume of all particles in the distribution. This data is then converted to a number-based (i.e., number per cubic centimeter) distribution by the following equation[24]

$$n_N(D_p) = \frac{6n_V(D_p)}{\pi D_p^3} \tag{1}$$

where D_p is the particle diameter in micrometers, and n_V is the volume-based distribution, which is equal to

$$n_V(D_p) = V_F \times V_T \tag{2}$$

where V_T is total volume concentration in parts per million (i.e., ratio of total volume of particles to total volume of air sampled), and V_F is the volume fraction (i.e., percent volume) of all particles within a particular size range in the total size distribution.

3.2 Meteorological optical range calculations

Metrics defining the transparency of the atmosphere are utilized in several domains such as aviation, meteorology, transportation, and shipping. The prominent metric was once termed "visual range" but has since become known as visibility.[28] Classically, visibility was a quantity that was determined subjectively by an observer. However, an alternative visibility metric exists today that

is quantitatively defined as the distance required to reduce the luminous flux of a collimated beam from a 2700K color temperature lamp to 5% of its original value. This metric is known as the Meteorological Optical Range (MOR). For the tests performed in this study, we utilize a MOR measurement to provide quantitative and repeatable measurements of the optical effects of fog on visible imager performance. The concepts of the MOR are founded on the Beer-Lambert law,[29] which states

$$I = I_0 e^{-\alpha d} \tag{3}$$

where I is the intensity of the measured target, I_0 is the nominal intensity, α is the attenuation coefficient, and d is the distance at which the source was located from the detector. Solving for α yields,

$$\alpha = \frac{ln\left(\frac{I}{I_0}\right)}{-d} \tag{4}$$

To calculate MOR, we define the ratio of the measured intensity to the nominal intensity as 5%. Mathematically, we define this as follows,

$$\frac{I}{I_0} = 0.05 = e^{-\alpha d_{MOR}} \tag{5}$$

Inserting equation 4 into equation 5, and solving for d yields the MOR (i.e., the distance at which intensity reduces to 5%)

$$d_{MOR} = d \times \frac{ln(0.05)}{ln\left(\frac{I}{I_0}\right)} \tag{6}$$

MOR measurements were implemented with a short baseline transmissometer configuration created using an LED white light as the emitter and a standard camera sensor as the photodetector. While not strictly conforming to the collimation and 2700K color temperature of the source, this configuration enables simple evaluation of optical degradations caused by scattering particulates using an unchanging source and sensor pair. Pixels within a known white and black target region of an optical test target were averaged to obtain intensity measurements. Nominal measurements were obtained without fog present in the fog chamber and used as the I_0 value. Knowledge of the target distance, I, and I_0 values enable the calculation of a relative MOR measurement compared to nominal, pre-fog conditions. As short baseline transmissometers are most accurate in the 4 m to 128 m range, all tests were implemented within these shorter distances.[30]

3.3 Relative spatial frequency response area under curve methods

Measurement of spatial frequency response (SFR) can be achieved via a number of methods.[31] We chose to utilize a sinusoidal Siemens star test target as described by the ISO 12233 photography resolution standard. Several works describe the usage of a sinusoidal Siemens test target and appropriate techniques to extract SFR from imagery. Motivation to utilize the sinusoidal Siemens star test rather than the more common slanted edge measurement is due to the presence of algorithmic edge enhancements applied to captured images from the camera tested. These edge enhancements artificially alter the contrast recorded by the camera at the slanted edge, and thus modify the SFR if slanted edge techniques are utilized. Previous work suggests the sinusoidal Siemens star test is less sensitive to artifacts induced by edge enhancement algorithms.[32]

However, the use of a sinusoidal Siemens star target can be complicated due to incorrect determinations of the test target center. Care must be taken to either precisely identify the center of the

test target using closed form mathematics for curve fitting of decentered radial sinusoid profiles, or by increasing the number of radial segments used to fit a sine wave to measured data.[33] In this analysis we utilized 64 sinusoidal Siemens star segments to mitigate errors due to misidentified target centers.

SFR AUC nominal measurements were taken before fog generation began. All subsequent SFR data was then normalized by the nominal set, and a trapezoidal numerical integration was performed to find the SFR AUC for every one second interval during a test. This method of normalization was used to account for imperfections in the imaging system or residual defocus that reduced the absolute SFR of the system at the beginning of a test, enabling direct measurement of the impact of atmospheric conditions on optical performance.

3.4 Proof of concept test method

A Lumenera Li165 color network surveillance camera was used to evaluate the effects of fog density on reported relative SFR AUC and MOR for different fog levels in the SNL fog chamber facility. The camera was placed in a weather proof casing and mounted on a tripod at the end of the fog tunnel. An open test target chamber with positive pressure housed an optical test target consisting of sinusoidal Siemens star targets and grayscale patches conforming to the ISO 12233 standard. The test target chamber contained two LED illumination sources oriented towards the test target. These light sources were the only illumination within the testing facility during the duration of a test. The camera was focused by visually maximizing the aliasing of the high frequency elements of the sinusoidal Siemens star test target at nominal, pre-fog conditions. Video was then recorded from the camera for the duration of a test, and frames were averaged together into one second intervals to match that of the Malvern Spraytech system. These one second interval datasets

were then utilized to calculate relative SFR AUC and MOR, as previously described.

Figure 2 (a) contains a diagram of the test setup, while figures 2 (b) through (d) show images of the test target captured by the camera with increasingly dense fog.

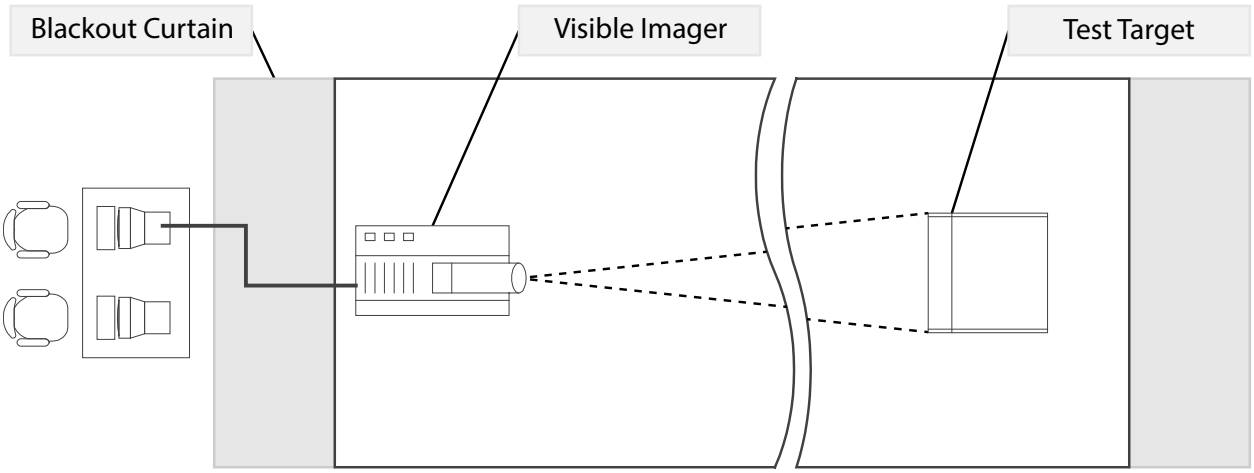

(a)

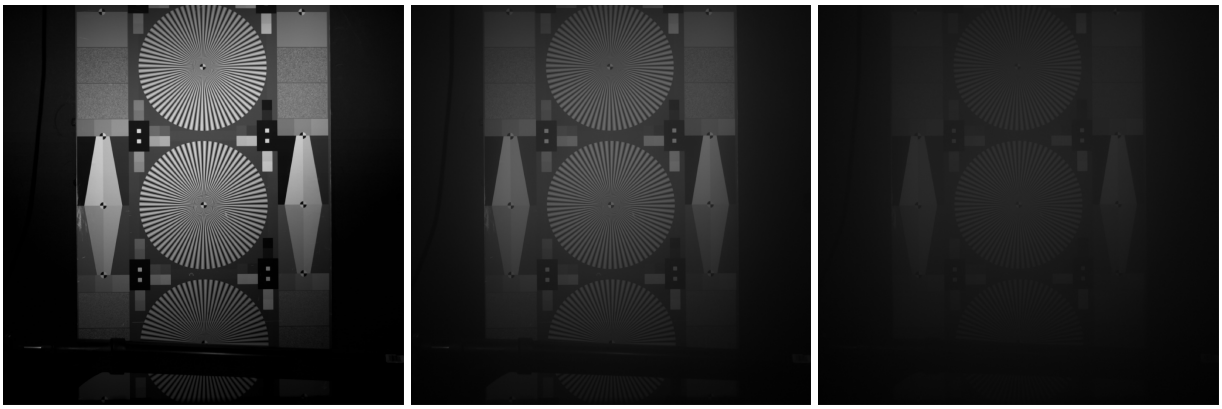

(b) (c) (d)

Fig 2 (a) Diagram of the SNL Fog Chamber and test configuration used in this study, (b) through (d), images captured by the Li165 camera with increasing fog density.

Nominal measurements were recorded from the camera for one minute, followed by fog generation and concurrent particle number measurements by the Malvern Spraytec instrument. Fog generation continued until fog density was so great that the test target became visually obscured. At this point, fog generation was stopped and natural dissipation of fog particles occurred.

This test procedure was repeated three times for test targets located at 10 feet, 20 feet, and 30

feet from the camera.

4 Results

4.1 Test One

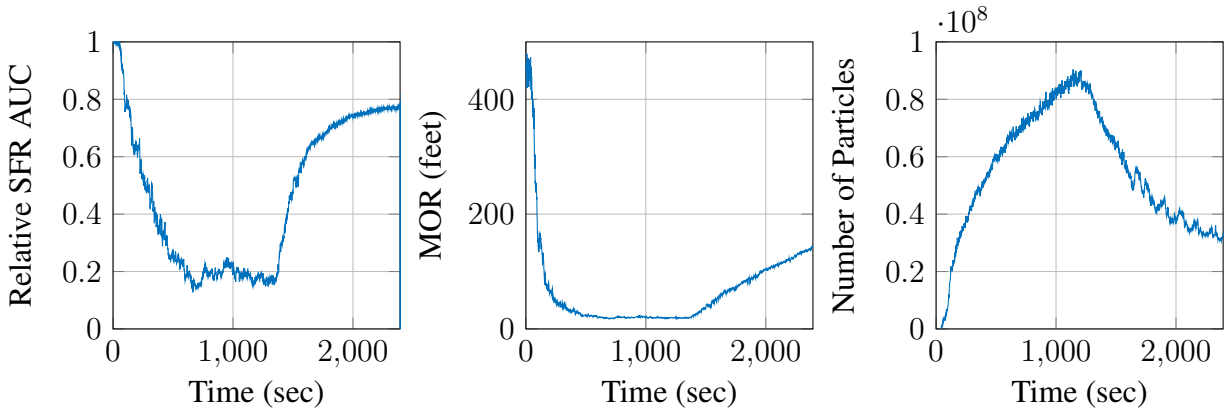

(a) (b) (c)

Fig 3 (a) Relative SFR AUC, (b) MOR, and (c) total number of particles in atmosphere. All data is plotted versus time, and measured during test one, which placed the ISO 12233 test target ten feet from the camera.

Test one placed the ISO 12233 test target approximately ten feet from the camera. Fog generation proceeded for approximately twenty minutes, until test target visibility was almost completely reduced, whereupon fog generation was halted. Fog dissipation began to reduce the total number of particles in the chamber.

Figure 3 (a) shows the recorded values of relative SFR AUC, figure 3 (b) shows MOR, and figure 3 (c) shows total number of particles in the atmosphere as measured by the Malvern Spraytec instrument. All values are a function of time, discretized into one second averages as described in the test methodology section.

Relative SFR AUC quickly decreased with the initial generation of fog particles, until a minimum value was reached within the 665 second to 1340 second period. Once fog generation was

stopped, relative SFR AUC rapidly increased for approximately 300 seconds, followed by a slower increase in relative SFR AUC for the remainder of the test.

Similarly, MOR rapidly decreased until a minimum value of approximately 17 feet was achieved between 500 seconds and 1375 seconds. After fog generation was stopped, MOR began a uniform and nearly-linear increase for the remainder of the test.

Total number of particles increased during fog generation. The average particle size distribution with a volume-based concentration was bimodal with peaks at 4.6 μm and 34 μm. However, when converted to a number-based distribution, the peak particle size was 1.4 μm. This indicates that, while large particles are present in the chamber, the majority of particles were small (i.e., <10 μm). Once fog generation stopped, particles naturally fell out of the atmosphere due to gravitational settling and evaporation affects which reduced the total number of particles over time. During fall out, the larger particles fall out of air faster than the smaller particles resulting in a non-linear decay in the number of particles present within the chamber.

4.2 Test Two

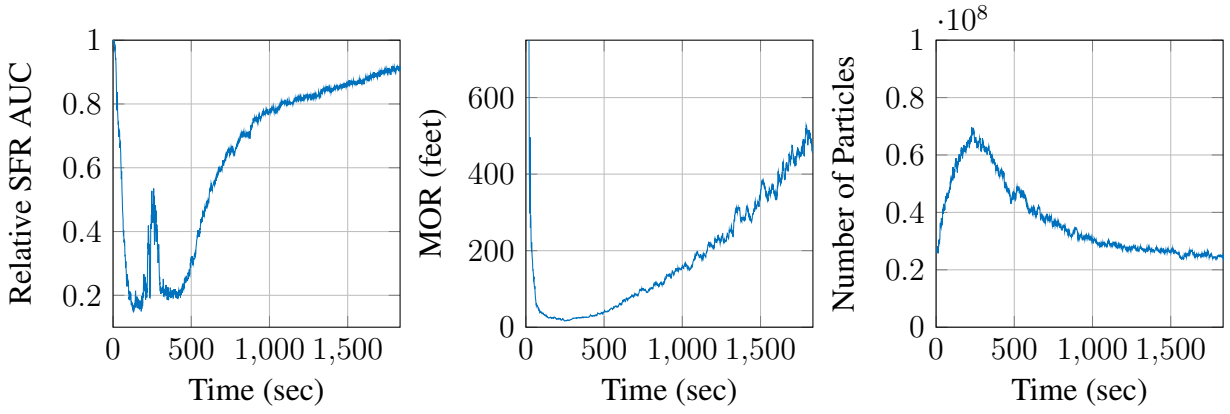

(a) (b) (c)

Fig 4 (a) Relative SFR AUC, (b) MOR, and (c) total number of particles in atmosphere. All data is plotted versus time, and measured during test two, which placed the ISO 12233 test target twenty feet from the camera.

Test two increased the distance to the ISO 12233 test target, placing the target approximately twenty feet from the camera. Figure 4 (a) through (c) show test results. Because the test target was located at a greater distance than test one, fewer number of particles were necessary to reduce the measured MOR. Fog generation proceeded for approximately 260 seconds. After fog generation halted, a decay in total number of particles occurred for the duration of the test, similar to that shown in Figure 3 (c).

A similar rapid recovery of relative SFR AUC began at approximately 450 seconds, followed by a period of slower recovery starting at 870 seconds. This test produced elevated relative SFR AUC measurements within time periods of MOR measurements less than the test distance. This spurious phenomenon occurs as an anomaly in the sinusoidal Siemens star curve fitting algorithm; very low signals produce meaningless SFR results that falsely elevate the recorded SFR.

MOR quickly decreased to values smaller than twenty feet. This would imply that less than 5% of the original intensity was being measured by the imager during the thickest fog. After fog generation was halted, MOR recovered similarly to figure 3 (b).

4.3 Test Three

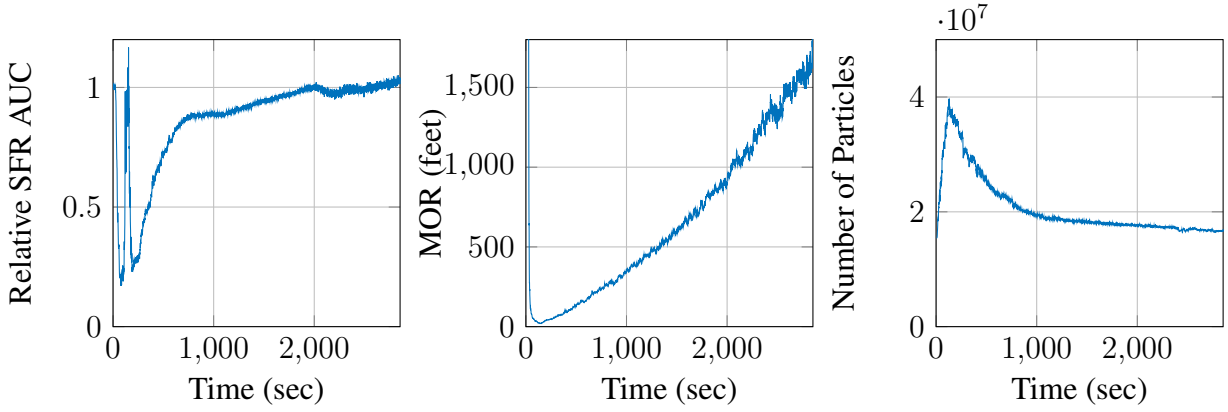

(a) (b) (c)

Fig 5 (a) Relative SFR AUC, (b) MOR, and (c) total number of particles in atmosphere. All data is plotted versus time, and measured during test three, which placed the ISO 12233 test target thirty feet from the camera.

Test three placed the ISO 12233 test target approximately thirty feet from the camera. Similar behavior to both test one and test two was shown, with fewer particles needed to reduced MOR due to comparatively larger optical path length. Test results are shown in figure 5. MOR rapidly declined to less than the test target distance, and increased near-linearly after fog generation was halted. The spurious relative SFR AUC region increased in value during times when MOR was extremely low, but showed a similar relative SFR AUC recovery after fog generation stopped, followed by a period of slower relative SFR AUC recovery for the duration of the test.

4.4 Discussion

Results obtained in tests one through three show generally similar behavior for number of particles versus time. Fewer particles were needed to reduce system performance as target distance increased, and particulate decay after fog generation was halted proceeded in a similar manner for each test. MOR measurements across each test showed a similar rapid decay as fog generation began, followed by a nearly-linear increase in MOR after fog generation was halted. However,

relative SFR AUC exhibited unexpected behavior; each test demonstrated a period of rapid relative SFR AUC recovery, followed by a slower recovery of relative SFR AUC. We hypothesize the relative SFR AUC metric is more susceptible to the presence of large particulates, and large particulates more rapidly fall out of the atmosphere due to gravitational settling when fog generation is suspended, causing the initial rapid recovery of relative SFR AUC.

5 Summary and Future Work

The Sandia National Laboratory Fog Chamber was demonstrated in a set of tests evaluating security camera relative SFR AUC, MOR, and number of particles in the chamber. Three tests were implemented within the test chamber at varying distances. Each test consisted of an ISO 12233 test target placed within the fog chamber and illuminated by two white light LEDs. Nominal data was obtained for each distance without fog. The chamber was then filled with fog until the test target was completely obscured. Fog generation was halted, and dissipation was allowed to occur. Imagery data and particle size data were measured during the entire period of fog generation and dissipation. Relationships between the MOR and fog particle number followed the general expected pattern in obscurants. However, relative SFR AUC was found to recover much faster than would be expected based off of MOR measurements. It is hypothesized that this initial period of increased recovery rate is due to rapid large particle fall out at the beginning of fog dissipation.

Future work will investigate relative SFR AUC, MOR, and number of particles in the atmosphere using different imaging systems. In particular, quantitative performance metrics in the long wave infrared (LWIR) are of interest to evaluate visible versus LWIR trade-offs in physical security systems. Additional work will investigate more complex constituents including chemical blends that mimic fog, smog, or haze caused by pollutants.

Funding

Sandia National Laboratories is a multi-mission laboratory managed and operated by Sandia Corporation, a wholly owned subsidiary of Lockheed Martin Corporation, for the U.S. Department of Energys National Nuclear Security Administration under contract DE-AC04-94AL85000. **SAND XYZ- Fill in with correct SAND number.**

Acknowledgments

We thank Steven Storch for assisting with tests that enabled this study.

References

1 E. Dumont, N. Hautiere, and R. Gallen, "A semi-analytic model of fog effects on vision," Research Gate (2010).

2 M. Colomb, K. Hirech, P. André, J. Boreux, P. Lacôte, and J. Dufour, "An innovative artificial fog production device improved in the european project "fog"," Atmospheric Research **87**, 242 – 251 (2008). Third International Conference on Fog, Fog Collection and DewFog and DewThird International Conference on Fog, Fog Collection and Dew.

3 H. Manor and S. Arnon, "Performance of an optical wireless communication system as a function of wavelength," Appl. Opt. **42**, 4285–4294 (2003).

4 J. Zeller and T. Manzur, "Effect of atmosphere on free-space optical communication networks for border patrol," (2010).

5 B. R. Strickland, M. J. Lavan, E. Woodbridge, and V. Chan, "Effects of fog on the bit-error rate of a free-space laser communication system," Appl. Opt. **38**, 424–431 (1999).

6 L. R. Bissonnette, "Imaging through fog and rain," Optical Engineering **31**, 1045–1052 (1992).

7 J. H. Taylor and H. W. Yates, "Atmospheric transmission in the infrared," J. Opt. Soc. Am. **47**, 223–226 (1957).

8 M. R. Clay and A. P. Lenham, "Transmission of electromagnetic radiation in fogs in the 0.53–10.1-μm wavelength range," Appl. Opt. **20**, 3831 1–3832 (1981).

9 D. G. Crowe, D. K. Cohen, and E. L. Dereniak, "Infrared propagation and performance modeling at the electro-optical test facility," Appl. Opt. **19**, 1953–1958 (1980).

10 J. C. Ramella-Roman, S. A. Prahl, and S. L. Jacques, "Three monte carlo programs of polarized light transport into scattering media: part ii," Opt. Express **13**, 10392–10405 (2005).

11 M. Grabner and V. Kvicera, "Multiple scattering in rain and fog on free-space optical links," J. Lightwave Technol. **32**, 513–520 (2013).

12 J. D. van der Laan, J. B. Wright, D. A. Scrymgeour, S. A. Kemme, and E. L. Dereniak, "Variation of linear and circular polarization persistence for changing field of view and collection area in a forward scattering environment," (2016).

13 J. D. van der Laan, D. A. Scrymgeour, S. A. Kemme, and E. L. Dereniak, "Range and contrast imaging improvements using circularly polarized light in scattering environments," (2013).

14 J. Han, K. Yang, M. Xia, L. Sun, Z. Cheng, H. Liu, and J. Ye, "Resolution enhancement in active underwater polarization imaging with modulation transfer function analysis," Appl. Opt. **54**, 3294–3302 (2015).

15 B. Ben-Dor, P. Bruscaglioni, A. D. Devir, P. Donelli, and A. Ismaelli, "Cloud, fog, and aerosol effect on the mtf of optical systems," (1995).

16 I. Gultepe, R. Tardif, C. S. Michaelides, J. Cermak, A. Bott, J. Bendix, D. M. Müller, M. Pagowski, B. Hansen, G. Ellrod, W. Jacobs, G. Toth, and G. S. Cober, "Fog research: A review of past achievements and future perspectives," Pure and Applied Geophysics **164**, 1121–1159 (2007).

17 E. Belin, F. Christnecher, F. Taillade, and M. Laurenzis, "Display of an analytical model for backscattered luminance and a full-field range gated imaging system for vision in fog," (2008).

18 V. Larochelle, D. Bonnier, G. Roy, J.-R. Simard, and P. Mathieu, "Performance assessment of various imaging sensors in fog," (1998).

19 H. G. Houghton, "The transmission of visible light through fog," Phys. Rev. **38**, 152–158 (1931).

20 J. Ruden, C. Wasser, S. Hulbert, and A. Burg, "Motorists requirements for active grade crossing warning devices," Tech. rep., US Department of Transportation Federal Highway Administration (1977).

21 D. K. Cohen, J. H. Hunt, and D. G. Crowe, "Characteristics of a chamber used for electrooptical device performance measurements in the presence of fog," Appl. Opt. **21**, 2399–2404 (1982).

22 A. Khlystov, G. Kos, and H. ten Brink, "A high-flow turbulent cloud chamber," Aerosol science and technology **24**, 59–68 (2012).

23 R. Gieray, P. Wieser, T. Engelhardt, E. Swietlicki, H.-C. Hansson, B. Mentes, D. Orsini, B. Martinsson, B. Svenningsson, K. Noone, and J. Heintzenberg, "Phase partitioning of

aerosol constituents in cloud based on single-particle and bulk analysis," Atmospheric Environment **31**, 2491 – 2502 (1997).

24 J. Seinfeld and S. Pandis, "Atmospheric chemistry and physics: From air pollution to climate change," (2016).

25 G. vanLoon and S. Duffy, "Environmental chemistry: A global perspective," (2011).

26 W. Hinds, "Aerosol technology: Properties, behavior, and measurement of airborne particles," (1999).

27 H. Hulst and H. van de Hulst, "Light scattering by small particles," (1957).

28 W. E. K. Middleton, "Vision through the atmosphere," pp. 254–287 (1957).

29 W. M. Organizati, "Guide to meteorological instruments and methods of observation," (2006).

30 D. G. D. J. M. O. W. S. W. M. O. W. I. V. I. 1st session (1988-1989; United Kingdom), "Wmo/td- no. 401; iom report- no. 41: The first wmo intercomparison of visibility measurements: final report," (1990).

31 I. O. for Standardization. Technical Committee Photography, "Iso-12233:2014 - photography: Electronic still-picture cameras - resolution measurements," (2014).

32 C. Loebich, D. Wueller, B. Klingen, and A. Jaeger, "Digital camera resolution measurement using sinusoidal siemens stars," (2007).

33 G. C. Birch and J. C. Griffin, "Sinusoidal siemens star spatial frequency response measurement errors due to misidentified target centers," Optical Engineering **54**, 074104 (2015).

Gabriel Birch is a scientist at Sandia National Laboratories. He received his PhD degree in optical sciences from the University of Arizona College of Optical Sciences in 2012. His current research

interest include physical security systems, testing and evaluation of imaging devices, and non-traditional imaging systems.

Andres Sanchez is a scientist at Sandia National Laboratories. He received his Master of Science degree in Chemical Engineering from the University of New Mexico in 2012. His current research includes atmospheric science, aerosol characterization, as well as, chemical and biological dissemination and decontamination.

Bryana Woo is an electronics engineer at Sandia National Laboratories. She recently received both her M.S. and B.S. in electrical engineering from the New Mexico Institute of Mining and Technology. Her work with Sandia National Laboratories has included modeling plasma physics, evaluating imaging systems, investigation of novel imaging devices, and implementing physical security systems.

Biography of the other author is not available.

List of Figures

List of Tables

None.